Advanced Composites and Hybrid Materials (2021) 4:725–732
https://doi.org/10.1007/s42114-021-00310-4

ORIGINAL RESEARCH

Adsorption of xanthate from aqueous solution by multilayer graphene oxide: an experimental and molecular dynamics simulation study

Lin Li[1] · Meng He[1] · Yanfei Feng[2] · Hengbin Wei[3] · Xiaofang You[1] · Hao Yu[1] · Qingbiao Wang[4] · JunXiang Wang[1]

Received: 29 March 2021 / Revised: 8 July 2021 / Accepted: 18 July 2021 / Published online: 28 July 2021

Abstract

Xanthate has become the main organic pollutant in mine wastewater because of its widespread use as a flotation collector. Multilayer graphene oxide (MGO) exhibits excellent adsorption performance in removing organic contaminants from aqueous solutions that is attributed to its rich oxygen-containing functional groups and large specific surface area. MGO was prepared using the modified Hummers method. Moreover, MGO was characterised by Raman spectroscopy, X-ray diffraction, and X-ray photoelectron spectroscopy (XPS). The adsorption of xanthate by MGO follows the Langmuir model, and thermodynamic studies have shown that the adsorption process can be completed spontaneously. The results of XPS analysis indicated that the oxygen content on the MGO surface decreased after the adsorption of xanthate, and the proportion of oxygen-containing functional groups was also significantly lower than that before adsorption. Molecular dynamics studies revealed that the head group of xanthates was closer to the surface of the MGO than the tail group. This research indicates that MGO can be successfully used to adsorb xanthate. In addition, the dispersion force between the head group of xanthates and the oxygen-containing functional group on the MGO surface was the dominant factor affecting the adsorption process.

Keywords Mine wastewater · Xanthate · Multilayer graphene oxide · Molecular dynamics · Adsorption

1 Introduction

Xanthate is one of the most effective and widely used collectors for the flotation of zinc, lead, nickel, copper, and sulphide minerals [1, 2]. Moreover, it is the main organic pollutant in mine wastewater since it is difficult to recycle and handle in ore dressing wastewater. Xanthate residues in water affect the survival of fish, reduces crop yield [3], and impairs the healthy functioning of the human nervous system and liver [4]. Therefore, it is crucial to remove residual xanthate from flotation wastewater.

Biodegradation [4–6], chemical oxidation [7, 8], and adsorption [9, 10] and other methods can remove xanthate from wastewater. However, the biological method is expensive and time-consuming. The oxidation method produces sulphide and causes secondary pollution. In contrast, the adsorption method is widely used and non-polluting, which is more suitable for the treatment of xanthate in flotation wastewater. Graphene oxide (GO) is one of the materials for the removal of pollutants, which has a better adsorption capacity due to the presence of numerous oxygen-containing polar groups, such as hydroxyl groups, epoxy groups, and carboxyl groups on both sides of the plane and the edge [11–13]. Many studies have revealed that GO has a good adsorption efficiency on heavy metal ions [14–16] and organic substances [17–19]. However, the research on the microscopic mechanism of GO to remove pollutants is not clear. Molecular dynamics (MD) connects macroscopic experimental phenomena and microscopic properties [20], which can be used to study the microscopic mechanism of adsorption. You et al. [21] investigated the adsorption of nonylphenol ethoxylate on GO in aqueous using solution

✉ JunXiang Wang
wangjunxiang1018@sdust.edu.cn

1 College of Chemical and Biological Engineering, Shandong University of Science and Technology, Qingdao 266590, China

2 Department of Resource and Environment, Moutai Institute, Renhuai 564500, China

3 Zhejiang Petroleum Branch, Sinopec Sales Co., Ltd, Hangzhou 310000, China

4 National Engineering Laboratory for Coalmine Backfilling Mining, Shandong University of Science and Technology, Tai'an 271019, Shandong, China

MD simulation; the research established that the polarity betwixt the ethoxylate group of nonylphenol ethoxylates and the oxygen-containing functional groups on the surface of GO was a major factor in the adsorption process.

Graphene oxide containing 10 layers and more is identified as multilayer graphene oxide (MGO), which possesses similar properties as single-layer graphene oxide and is easier to manufacture. In this study, MGO is used to remove xanthate from wastewater. The effects of temperature and xanthate concentration on adsorption properties are investigated, and the adsorption mechanism is studied via MD simulation, which can provide theoretical guidance for the application of MGO in the treatment of xanthate wastewater.

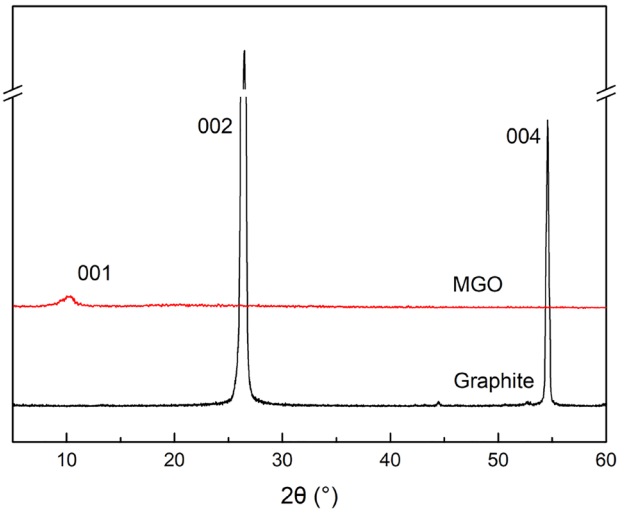

Fig. 1 XRD pattern of graphite and MGO

2 Materials and methods

2.1 Materials

Graphite was purchased from Qingdao Tianshengda Graphite Co., Ltd. (China); its size was greater than 0.149 mm and was 99.9% pure. n-Butyl xanthate (industrial grade) was purchased from Qingdao Chemical Reagent Co., Ltd. (China). Phosphorus pentoxide (P_2O_5), potassium permanganate ($KMnO_4$), and potassium persulphate ($K_2S_2O_8$) were purchased from Tianjin Komiou Chemical Reagent Co., Ltd. (China). Hydrogen peroxide (H_2O_2) (30 wt%), sulphuric acid (H_2SO_4), phosphoric acid (H_3PO_4), and hydrochloric acid (HCl) were purchased from Chengdu Chron Chemical Co., Ltd. (China). Anhydrous ethanol was purchased from Tianjin Fuyu Fine Chemical Co., Ltd. (China). All chemicals were of analytical grade and used without further purification.

2.2 Methods

2.2.1 Preparation of MGO

Graphite oxide was prepared using the modified Hummers method [22, 23]. Graphite (1 g) was added to a beaker containing 40 mL of a sulphur–phosphorus mixed acid for pre-oxidation. Subsequently, 4 g of $KMnO_4$ was added to the pre-oxidised graphite and stirred for 45 min in an ice bath. Additionally, the mixture was stirred for 2 h at 35 °C and then stirred for 1 h at 70 °C. Next, 100 mL of distilled water and 17 mL of H_2O_2 were slowly added to the mixture and stirred for 15 min. The solid–liquid mixture was separated by centrifugation, and the solid deposit was washed with hydrochloric acid until the supernatant was free of SO_4^{2-}. Furthermore, the precipitate was washed with distilled water until the supernatant was neutral, followed by ultrasonic dispersion in distilled water for 15 min. Finally, the graphite oxide solution was dried in a vacuum freeze-drying cabinet. The XRD and Raman spectroscopy patterns of graphite and MGO are shown in Figs. 1 and 2, respectively.

The characteristic peak (002) corresponding to graphite appears at $2\theta = 26.48°$, and according to the Bragg equation, the spacing of the graphite layers was calculated to be 0.34 nm. The characteristic (002) peak disappeared completely in the MGO patterns. The diffraction peak of MGO was observed at $2\theta = 10.34°$, and the spacing of layers was 0.91 nm. Moreover, the BET specific surface area of MGO was 163.35 m^2/g. It follows that the MGO was successfully prepared [24].

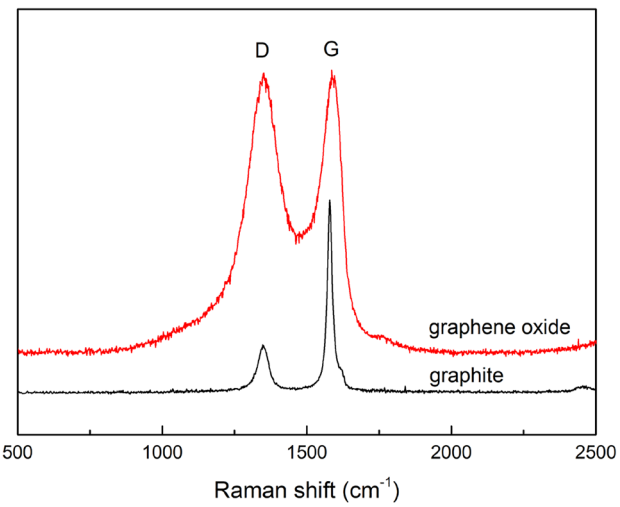

Fig. 2 Raman spectrum of graphite and MGO

2.2.2 Testing methods

XRD patterns with a scan range of 10–90° were obtained from X'pert Pro MPD (Rigaku, model Max2500PC) with Cu Kα radiation (100 mA, 40 kV) at a scan rate of 5°/min and a step size of 0.02° [25]. The Raman spectra of the films in a HORIBA Scientific HR Evolution reactor under atmospheric conditions were collected using 532-nm excitation wavelength at room temperature (298 K). The oxygen-containing function analysis on the surface of graphite oxide and its specific surface area are carried out by a Thermo Fisher Scientific ESCALAB 250 spectrometer [26] and an ASAP 22460 analyser from Micromeritics, respectively.

After adding 0.02 g of MGO to an Erlenmeyer flask with 100 mL of xanthate solution, the flask was shaken for 2 h in a water bath maintained at a specific temperature. The mixture was subsequently filtered through a microfiltration membrane (0.45 μm) to obtain the filtrate, and the absorbance was measured at 301 nm using an Agilent CARY 60 spectrophotometer; the concentration of xanthate after adsorption was calculated based on the standard curve. The equilibrium adsorption capacity can be calculated using the formula in the literature [21, 27].

2.2.3 Molecular dynamics simulation

The Forcite module of Materials Studio 8.0 was used for molecular dynamics simulations. First, a model of MGO and xanthate (sodium n-butyl xanthate) was built, and the MGO model was constructed based on the XPS analysis results [28]. Moreover, the molecular formula of MGO is $C_{29}O_3(OH)_3(COOH)_2$, and the carbon atom consists of sp^2 hybridised carbon, hydroxyl groups, carboxyl groups, and epoxy groups. The sp^2 hybridised carbon was treated as uncharged Lennard-Jones spheres. The electric charges of the epoxy, hydroxyl, and carboxyl groups in the MGO model and each atom in xanthate are shown in Table 1. The models of MGO and xanthate are shown in Fig. 3.

A rectangular simulation cell of MGO with three-dimensional perimeter conditions of 39.5 × 29 × 100 Å ($X \times Y \times Z$) was built using an amorphous cell module containing 4 xanthate and 1000 water molecules (SPC model). The optimisation and simulation were performed in two stages. During the first stage, constant pressure–temperature (NPT) time integration was performed using a Berendsen barostat and a Nosé–Hoover thermostat for 1 ns. Subsequently, a vacuum slab was added to the top of the system, and ensuing molecular dynamics simulations were performed using the Nosé–Hoover thermostat in the canonical (NVT) ensemble. The temperature was 298.15 K, the simulation time was 10 ns, the van der Waals interaction cut-off was 12.5 Å, and the time step was 1.0 fs. The simulation of 5 ns after the balance period was the foundation of the ultimate calculation results.

Table 1 Electric charge of multilayer graphene oxide and n-butyl xanthate molecule

Type	Molecule	Site	$Q(e)$
MGO	sp^2 hybridised carbon	C	0.0
	Epoxy	C	+0.2
		O	−0.4
	Hydroxyl	C	+0.1966
		O	−0.526
		H	+0.3294
	Carboxyl	C	+0.55
		O	−0.5
		O	−0.58
		H	0.45
Xanthate		Na	+1.0
	Normal-butyl	C	−0.159
		H	−0.053
	Xanthogenate	O	−0.186
		C	+0.1
		S	−0.242
		S	0.0

The polymer consistent force field (PCFF) of the Forcite module was used in the MD simulations. In the PCFF, the potential energy can be expressed as [29]:

$$E_{\text{total}} = E_{\text{valence}} + E_{\text{cross - term}} + E_{\text{non - bond}} \quad (1)$$

E_{valence} is the valence energy, which has a bond stretching term, an angle term, a torsion term, and an out-of-plane term. The $E_{\text{cross-term}}$ is a cross-term that illustrates the special effects such as bond lengths and angle changes caused by the adjacent atoms. $E_{\text{non-bond}}$ are non-bond terms that explain the interaction between non-bonded atoms, which include van der Waals energy and Coulomb electrostatic interactions. The PCFF uses different terms for various components of the potential [30].

3 Results and discussion

3.1 Adsorbent isotherm

The adsorption isotherms of xanthate on MGO at 283, 293, 303, and 313 K are presented in Fig. 4. Under different temperature conditions, the equilibrium adsorption amount of MGO to xanthate increased with increasing concentration of the xanthate solution. The reason for this phenomenon may be that the increase in temperature

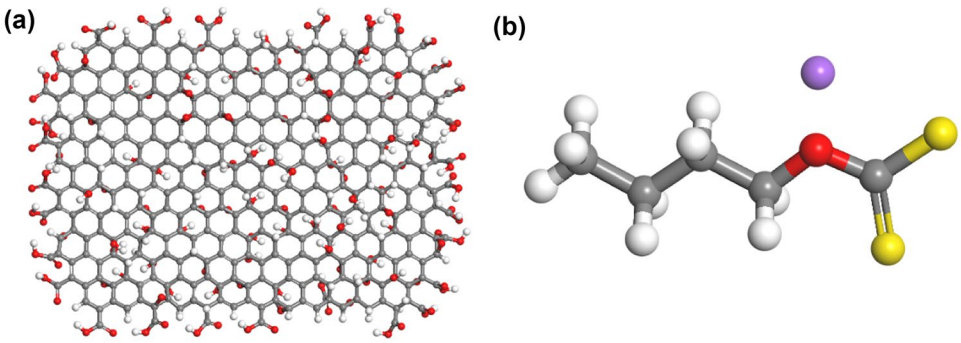

Fig. 3 Images of the top view of MGO (**a**) and xanthate (**b**). Coloured spheres represent O (red), C (grey), H (white), S (yellow), and Na (purple) for clarity

improved the availability of the adsorbent surface, which led to an increase in the diffusion rate of xanthate [31].

The experimental results were simulated using the Langmuir isotherm adsorption models [32–34]. The adsorption curves and parameters are presented in Table 2. The correlation coefficient R^2 obtained by the Langmuir equation exceeded 0.99, indicating that the adsorption of xanthate by MGO was consistent with the Langmuir isotherm adsorption model. Additionally, the maximum adsorption amount at different temperatures increased with an increase in temperature. Meanwhile, the maximum adsorption amount was significantly higher than that of modified bentonite activated under similar conditions [10]. This phenomenon occurs because MGO is a sheet-like material with an ultrahigh specific surface area rich in functional groups, resulting in a large amount of xanthate adsorbed onto the MGO.

To further investigate the adsorption characteristics of xanthate on MGO, the thermodynamic parameters, such as Gibbs free energy ΔG, enthalpy change ΔH, and entropy change ΔS were calculated using formulas (2),(3),(4) [35].

$$\Delta G = -RT \ln K \tag{2}$$

$$d \ln K / d(1/T) = -\Delta H / R \tag{3}$$

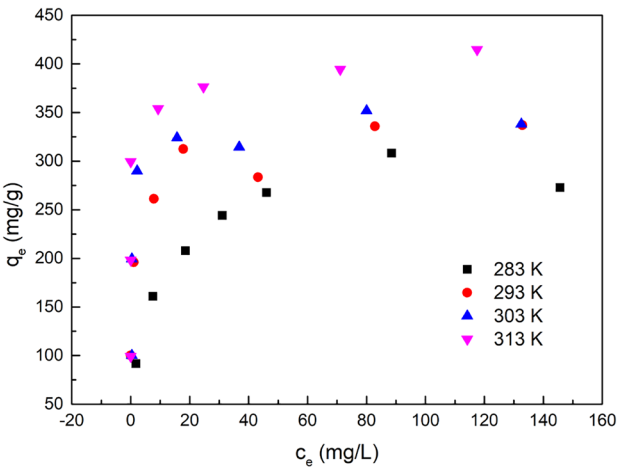

Fig. 4 Adsorption isotherm curve of MGO for xanthate

$$\Delta G = \Delta H - T\Delta S \tag{4}$$

where $R = 8.314$ J (mol K)$^{-1}$, which is the molar gas constant; K is a constant that can be obtained from the Langmuir adsorption model parameter, and T is the absolute temperature, kelvin. The calculation outcomes are presented in Table 3.

It can be observed from Table 3 that the ΔG of the xanthate adsorption by MGO is negative, suggesting that adsorption can occur spontaneously. Moreover, with an increase in temperature, the absolute value of ΔG gradually increased, indicating that the temperature increase was beneficial to the adsorption process. The adsorption enthalpy change ΔH is positive and less than 40 kJ mol^{-1}, indicating that the adsorption of xanthate on MGO is endothermic and related to physical adsorption. ΔS is greater than zero, indicating that the adsorption process increases the entropy, mainly because the xanthate molecules replace the water molecules adsorbed on the surface of the MGO, causing closely arranged water molecules on the surface of the MGO to transform into free moving molecules in the solution, thereby increasing the chaos of the whole system.

Table 2 Parameters of the Langmuir adsorption model

T, K	q_{max}, mg g^{-1}	K_L, L mg^{-1}	R^2
283	291.5452	0.2152	0.99078
293	340.1361	0.4428	0.99587
303	359.7122	1.8912	0.99988
313	411.5226	0.9798	0.99896

Table 3 Thermodynamic parameters of MGO adsorption for n-butyl xanthate

T, K	ΔG, kJ mol^{-1}	ΔH, kJ mol^{-1}	ΔS, J (mol K)$^{-1}$
283	−24.75	30.79	197.55
293	−27.39	30.79	198.54
303	−30.88	30.79	203.53
313	−31.32	30.79	198.43

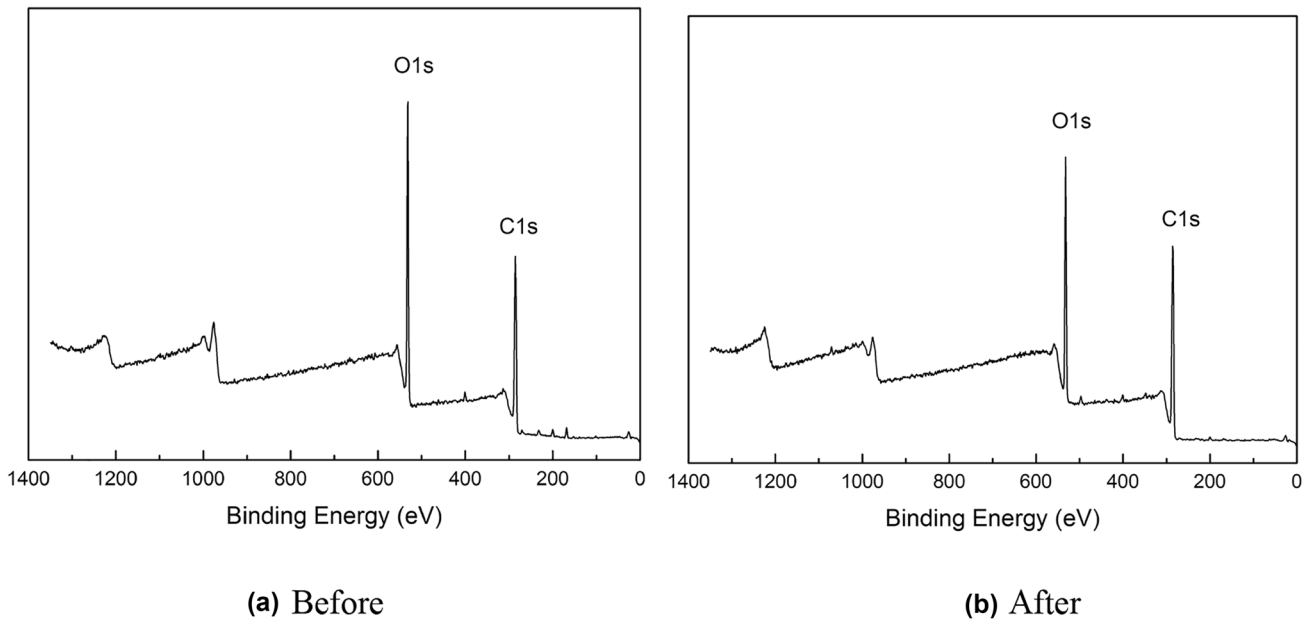

Fig. 5 XPS survey scans of xanthate adsorption on the MGO surface: **a** before; **b** after

3.2 Adsorption mechanism

XPS provides information on the surface chemistry of MGO before and after the adsorption of xanthate [36]. Fig. 5 shows the XPS wide-scan spectrum of MGO before and after adsorption of xanthate, and the relative content analyses of surface elements are listed in Table 4. The oxygen content on the surface of MGO decreased from 34.88% before adsorption to 29.28% after adsorption, which is attributable to the attachment of by xanthate to the oxygen-containing functional groups on the MGO surface. Moreover, the oxygen content in xanthate was lower than that in MGO. This also confirms that MGO can be successfully used to adsorb xanthate [34, 35, 37].

The results of the C 1s spectra of MGO before and after adsorbing xanthate are shown in Fig. 6, and the relative contents of the functional groups are listed in Table 5. The total content of –COOH, C=O, and C–O was higher than that of C–C, which clearly reflected the high oxidation degree of MGO. The –COOH content was significantly lower than that before adsorption, indicating that the active oxygen-containing groups can provide necessary adsorption sites for xanthate.

3.3 MD simulations

The simulation snapshots of xanthate adsorbed on the MGO surface at various simulation times are shown in Fig. 7. The xanthate molecules are placed on the surface of the MGO. As observed in Fig. 7b, the adsorption reaction is dominated by electrostatic repulsion at this time, and the xanthate molecules begin to move away from the MGO superficies. As the simulation progressed (Fig. 7c, d), the xanthate molecules gradually deformed and showed a tendency to be gradually adsorbed on the surface of MGO. The simulation snapshots indicate (Fig. 7d–f) that the structural characteristics remain mostly invariable from 1 ns. It was demonstrated that the head group of the xanthate molecule was adsorbed on to the surface of MGO and the tail group faces the water, which meant that the electrostatic interaction between the head base of xanthate and MGO is greater than the van der Waals force interaction between the tail base and MGO [37, 40].

As shown in Fig. 8, the *Z*-axis density profiles for the head and tail groups of the xanthate were analysed. The maxima of head and tail groups appeared at 15.4 Å and 16.1 Å, respectively, indicating that the hydrophilic head group is more proximal to the MGO surface than its hydrophobic tail group. This signifies that the van der Waals force is stronger between the xanthogen group and the hydrophilic site of the MGO surface. The deformability of xanthate increased as the adsorption progressed, leading to an increase in the dispersion force between the head group and MGO. An implication of this is that the dispersion force is the dominant

Table 4 Contents of C 1s and O 1s on the MGO surface

Types	Before		After	
	BE, eV	Atom, %	BE, eV	Atom, %
C 1s	284.6	65.12	284.6	70.42
O 1s	541.8	34.88	532.39	29.28

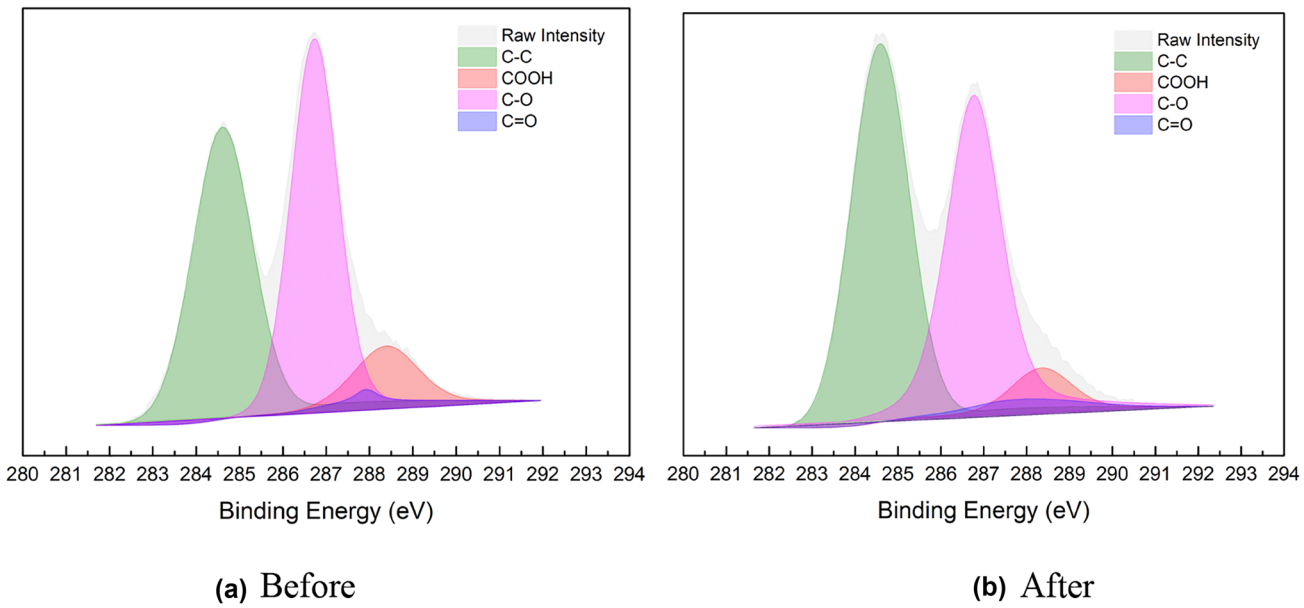

Fig. 6 C 1s spectra for MGO adsorbed with xanthate: **a** before; **b** after

Table 5 Fitting results of C 1s for graphite oxide

Groups	C–C	COOH	C=O	C–O
Before	45.21	9.04	1.14	44.61
After	48.80	4.96	2.18	44.06

force affecting the process of xanthate adsorption by MGO. This inference is supported by the observations in Fig. 7 that the head group is preferentially adsorbed on the hydrophilic site of MGO, while the hydrophobic tail group is exposed to the solution.

The mean square displacement (MSD) curves of the head and tail groups in xanthate around MGO are presented in Fig. 9, and the self-diffusion coefficient (D), which represents the intensity of atomic migration, can be used to assess the mobility of the head and tail groups in xanthate around MGO. The value of D is calculated using Einstein's equation [38, 39], and the relationship between D and MSD is presented as follows:

$$D = \lim_{x\to\infty}\left(\frac{\mathrm{MSD}}{6t}\right) = \frac{1}{6}K_{\mathrm{MSD}} \tag{5}$$

The self-diffusion coefficients of head and tail groups were 5.19×10^{-6} cm^2/s and 5.40×10^{-6} cm^2/s, respectively, indicating that the mobility of the tail group was greater than that of the head group. The base of the head is fixed to the MGO surface because of the effect of the dispersion force; thus, the tail group migrates more easily and stays away from the MGO surface.

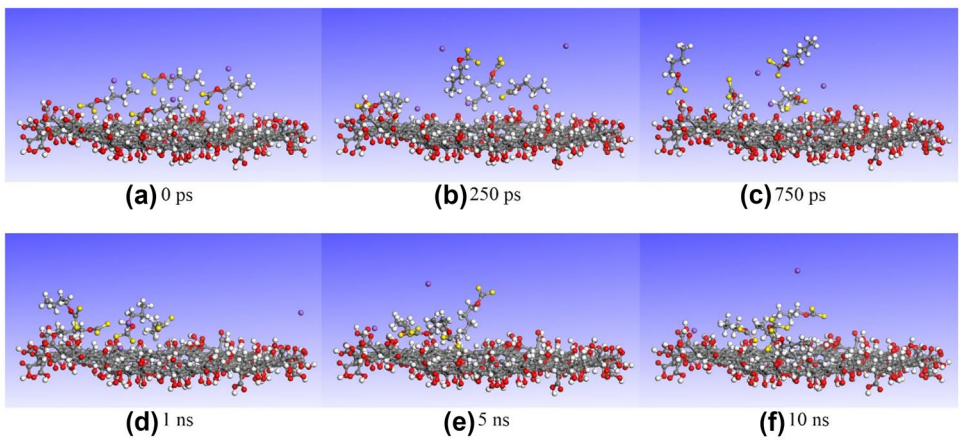

Fig. 7 Simulation snapshots of xanthates on MGO surface at varying simulation times: **a** 0 ps; **b** 250 ps; **c** 750 ps; **d** 1 ns; **e** 5 ns; **f** 10 ns

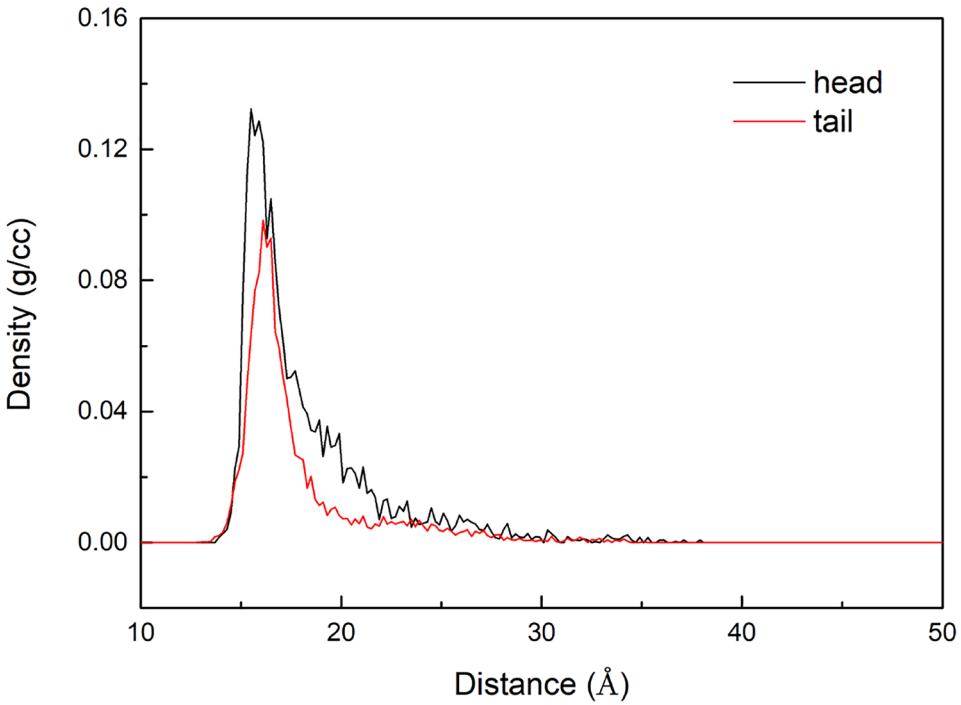

Fig. 8 Head and tail group density distributions of the xanthates along *Z*-axis direction

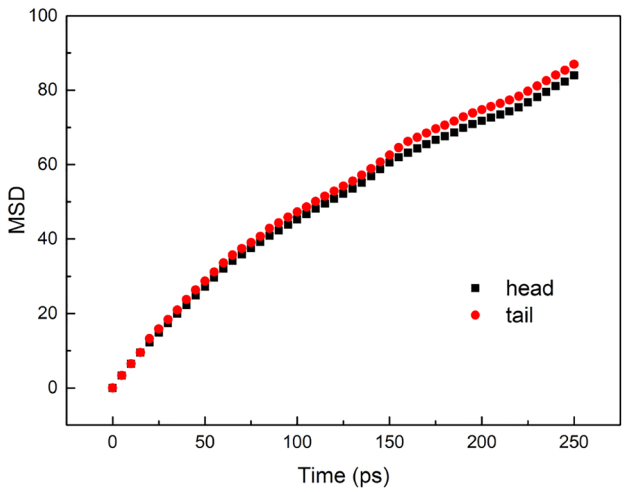

Fig. 9 Mean square displacement curves of head and tail groups of xanthates around MGO

4 Conclusions

In this paper, MGO rich in oxygen-containing functional groups and a typical two-dimensional fold structure was prepared, and the adsorption performance and mechanism for xanthate in wastewater were studied. Adsorption experiments showed that the adsorption of xanthate on MGO followed the Langmuir adsorption model. Thermodynamic calculations revealed that the adsorption of xanthate on the surface of MGO is a spontaneous endothermic process, which belongs to physical adsorption. XPS research showed that the active oxygen-containing groups can provide necessary adsorption sites for xanthate. Molecular dynamics simulation studies indicated that the hydrophilic head group of xanthate molecules is more proximal to the MGO superficies than the hydrophobic tail group. The excellent adsorption performance makes MGO one of the excellent adsorbents for removing xanthate in wastewater.

Funding This work was supported by the National Natural Science Foundation of China (Nos. 51904174, 52074175), Natural Science Foundation of Shandong Province (No. ZR2019BEE075), Young Science and Technology Innovation Program of Shandong Province (No. 2020KJD001), Key Research and Development Project of Shandong (No. 2019GGX103035), Scientific Research Foundation of Shandong University of Science and Technology for Recruited Talents (No. 2019RCJJ007), and Youth Science and Technology Talent Growth Program of Guizhou Province (No. KY[2018]466).

Declarations

Conflict of interest The authors declare no competing interests.

References

1. Hope GA, Watling K, Woods R (2001) A SERS spectroelectrochemical investigation of the interaction of isopropyl, isobutyl and isoamyl xanthates with silver. Colloids and Surfaces A: Physicochem Eng Aspects 178(1–3):157–66.
2. Liu W, Liu W, Wang B, Duan H, Zhao Q (2019) Novel hydroxy polyamine surfactant N-(2-hydroxyethyl)-N-dodecyl-ethanediamine: its synthesis and flotation performance study to quartz. Min Eng 142:105894.

3. Molina GC, Cayo CH, Rodrigues MANS, Bernardes AM (2013) Sodium isopropyl xanthate degradation by advanced oxidation processes. Minerals Eng 45:88–93.
4. Fu P, Feng J, Yang T, Yang H (2015) Comparison of alkyl xanthates degradation in aqueous solution by the O_3 and UV/O_3 processes: efficiency, mineralization and ozone utilization. Minerals Engineering. 81:128–34
5. Cheng W, Zhang Q, Wen-Qiang MA (2010) A research on removal of xanthate from floatation wastewater with activated carbon. Acta Mineralogica Sinica 30(2):262–7
6. Liu R, Sun W, Ouyang K, Zhang L, Hu Y (2015) Decomposition of sodium butyl xanthate (SBX) in aqueous solution by means of OCF: ozonator combined with flotator. Minerals Eng 70:222–7.
7. Chockalingam E, Subramanian S, Natarajan KA (2003) Studies on biodegradation of organic flotation collectors using Bacillus polymyxa. Hydrometallurgy 71(1–2):249–56
8. Chen S, Gong W, Mei G, Zhou Q, Bai C, Xu N (2011) Primary biodegradation of sulfide mineral flotation collectors. Minerals Engineering 24(8):953–5
9. Rezaei R, Massinaei M, Zeraatkar Moghaddam A (2018) Removal of the residual xanthate from flotation plant tailings using modified bentonite. Minerals Eng 119:1–10.
10. Amrollahi A, Massinaei M, Moghaddam AZ (2019) Removal of the residual xanthate from flotation plant tailings using bentonite modified by magnetic nano-particles. Minerals Eng 134(142–55):11.
11. Lerf A, He H, Forster M, Klinowski J (1998) Structure of graphite oxide revisited. The Journal of Physical Chemistry B. 102(23):4477–82
12. Dreyer DR, Park S, Bielawski CW, Ruoff RS (2009) The chemistry of graphene oxide. Chem Soc Rev 39(1):228–40.
13. Fallah S, Mamaghani HR, Yegani R, Hajinajaf N, Pourabbas B (2020) Use of graphene substrates for wastewater treatment of textile industries. Adv Compos Hybrid Mater 3(3):1–7.
14. Kommu A, Velachi V, Cordeiro MNDS, Singh JK (2017) Removal of Pb(II) Ion using PAMAM dendrimer grafted graphene and graphene oxide surfaces: a molecular dynamics study. J Phys Chem A. 121(48):9320–9.
15. Chandra V, Kim KS (2011) Highly selective adsorption of Hg^{2+} by a polypyrrole-reduced graphene oxide composite. Chem Commun 47(13):3942–4.
16. Mi X, Huang G, Xie W, Wang W, Liu Y, Gao J (2012) Preparation of graphene oxide aerogel and its adsorption for Cu^{2+} ions. Carbon. 50(13):4856–64
17. Xu J, Wang L, Zhu Y (2012) Decontamination of bisphenol A from aqueous solution by graphene adsorption. Langmuir 28(22):8418–25.
18. Xu J, Zhu Y-F (2013) Elimination of bisphenol A from water via graphene oxide adsorption. Acta Physico-Chimica Sinica 29(04):829–36.
19. Zhang Y, Cheng Y, Chen N, Zhou Y, Li B, Gu W, Shi X, Xian Y (2014) Recyclable removal of bisphenol A from aqueous solution by reduced graphene oxide–magnetic nanoparticles: adsorption and desorption. J Colloid Interface Sci 421:85–92.
20. Liu W, Liu W, Wang B, Zhao Q, Chen X (2019) Molecular-level insights into the adsorption of a hydroxy-containing tertiary amine collector on the surface of magnesite ore. Powder Tech 355:700–7.
21. You X, He M, Cao X, Wang P, Wang J, Li L (2019) Molecular dynamics simulations of removal of nonylphenol pollutants by graphene oxide: experimental study and modelling. Appl Surf Sci 475:621–6.
22. Singh M, Bajaj NK, Bhardwaj A, Singh P, Kumar P, Sharma J (2018) Study of photocatalytic and antibacterial activities of graphene oxide nanosheets. Adv Compos Hybrid Mater 1(4):759–65.
23. Singh N, Jana S, Singh GP, Dey RK (2020) Graphene-supported TiO_2: study of promotion of charge carrier in photocatalytic water splitting and methylene blue dye degradation. Adv Compos Hybrid Mater 3(1):127–40.
24. Zhang W, Shi X, Zhang Y, Gu W, Li B, Xian Y (2013) Synthesis of water-soluble magnetic graphene nanocomposites for recyclable removal of heavy metal ions. J Mater Chem A. 1(5):1745–53
25. Liu Q, Yang C, Lyu X, Chen P, You X, Li L, Wang J (2021) Evolution of ettringite content and its effects on hydration properties of CaO/fluorgypsum-activated granulated blast furnace slag binders. Adv Comp Hybrid Matl.
26. Zhang X, Ziemer KS, Weeks BL (2019) Combustion synthesis of N-doped three-dimensional graphene networks using graphene oxide–nitrocellulose composites. Adv Compos Hybrid Mater 2(3):492–500.
27. Liu S, Chen M, Cao X, Li G, Zhang D, Li M, Meng N, Yin J, Yan B (2020) Chromium (VI) removal from water using cetylpyridinium chloride (CPC)-modified montmorillonite. Sep Purifi Tech 241:116732.
28. Zhang W, He M, Wei H, Zhu X, You X, Lyu X, Li L (2018) Molecular dynamics simulations of interaction between subbituminous coal and water. Mol Simul 44(9):769–73
29. Plimpton S (1995) Fast parallel algorithms for short-range molecular dynamics. J Comput Phys 117(1):1–19.
30. Sun HJ (1998) COMPASS: an ab initio force-field optimized for condensed-phase applications – overview with details on alkane and benzene compounds. J Phys Chem B 102:7338–64.
31. Gao Y, Li Y, Zhang L, Huang H, Hu J, Shah SM, Su X (2012) Adsorption and removal of tetracycline antibiotics from aqueous solution by graphene oxide. J Colloid Interface Sci 368(1):540–6
32. Xiang X, Pan F, Li Y (2017) A review on adsorption-enhanced photoreduction of carbon dioxide by nanocomposite materials. Adv Compos Hybrid Mate 1(1):6–31.
33. He M, Zhang W, Cao X, You X, Li L (2018) Adsorption behavior of surfactant on lignite surface: a comparative experimental and molecular dynamics simulation study. Int J Mol Sci 19(2):437.
34. Yu G, Lu Y, Guo J, Patel M, Bafana A, Wang X, Qiu B, Jeffryes C, Wei S, Guo Z (2018) Carbon nanotubes, graphene, and their derivatives for heavy metal removal. Adv Compos Hybrid Mater 1:56–78.
35. Lyu X, You X, He M, Zhang W, Wei H, Li L, He Q (2018) Adsorption and molecular dynamics simulations of nonionic surfactant on the low rank coal surface. Fuel. 211:529–34
36. Gang Z, Cuicui X, Weimin C, Qi Z, Wen N (2015) Effects of oxygen element and oxygen-containing functional groups on surface wettability of coal dust with various metamorphic degrees based on XPS experiment. J Anal Method Chem 2015:467242.
37. You X, He M, Zhu X, Wei H, Cao X, Wang P, Li L (2019) Influence of surfactant for improving dewatering of brown coal: a comparative experimental and MD simulation study. Sep Purifi Tech 210:473–8.
38. Tao C, Feng H, Zhou J, Lu L, Lu X (2009) Molecular simulation of oxygen adsorption and diffusion in polypropylene. Acta Physico-Chimica Sinica. 25(7):1373–8
39. You X, He M, Zhang W, Wei H, Lyu X, He Q, Li L (2018) Molecular dynamics simulations of nonylphenol ethoxylate on the Hatcher model of subbituminous coal surface. Powder Tech 332:323–30
40. Zhang Y, Zhu H, Zhu J, Yang F, He H, Qin Z, Shi Q, Pan G (2021) Experimental and emulational study on the role of ion in coal adsorbing kerosene: Water-kerosene interface and catenoid characteristics. Fuel. 294: 120540.